Genesis locations of the costliest atmospheric rivers impacting the Western United States

Hamish D. Prince[1*], Peter B. Gibson[1], Michael J. DeFlorio[1], Thomas W, Corringham[1], Alison Cobb[1], Bin Guan[2,3], F. Martin Ralph[1] and Duane E. Waliser[2,3]

[1]Center for Western Weather and Water Extremes, Scripps Institution of Oceanography, University of California, San Diego, La Jolla, CA, USA,

[2]Jet Propulsion Laboratory, California Institute of Technology, Pasadena, CA, USA,

[3]Joint Institute for Regional Earth System Science and Engineering, University of California, Los Angeles, CA, USA

**Corresponding author*: Hamish Prince, prince.hamishd@gmail.com

Key Points:

- Historical flood damages from the Western U.S. are paired with an atmospheric river lifecycle tracking algorithm
- Damaging atmospheric rivers tend to have genesis locations further from the coastline, travel further and have a higher moisture flux
- The genesis of damaging atmospheric rivers is associated with distinct dipole pressure anomalies paired with an elevated zonal jet stream

Word count (including figure captions): 3,974

Word limit:4,000

Four Figures

Abstract

Atmospheric rivers (ARs) are responsible for the vast majority (approximately 88%) of flood damage in the Western U.S, an annual average of USD$1.1 billion. Here, using historical flood insurance data, we investigate the genesis characteristics of damaging ARs in the Western U.S. ARs exceeding USD$20 million in damage ($90^{th}$ percentile), are shown to travel further across the Pacific Ocean, with median genesis locations 8° to 27° longitude further westward compared to typical ARs. Identifying regions of preferential genesis of damaging ARs elicit important implications for AR observation campaigns, highlighting distant regions not currently considered for AR reconnaissance. The genesis of damaging ARs is associated with elevated upper-level zonal wind speeds along with deeper cyclonic anomalies, most pronounced for Washington and Oregon ARs. Linking AR dynamics and lifecycle characteristics to economic damage provides an opportunity for impact-based forecasting of ARs prior to landfall, supporting efforts to mitigate extreme flood damages.

Plain Language Summary

We examine the economic impact of atmospheric rivers, corridors or elevated atmospheric moisture vapor transport, on the Western U.S. Atmospheric rivers are responsible for the vast majority of flood damage which is experienced in the Western U.S. causing mean annual damages of USD$1.1 billion, 88% of the total annual flood damage. We use 40 years of historic flood insurance claims paired with a database of all atmospheric rivers that make landfall on the U.S. West Coast to show, for the first time, the relationship between atmospheric river dynamics and the economic impact for the Western. U.S. Our results show that damaging atmospheric rivers tend to originate further from the U.S. coastline than all other, less damaging atmospheric rivers. We also demonstrate the atmospheric conditions favourable for the initiation of damaging atmospheric rivers with a particular focus on atmospheric rivers that travel across the entire Pacific Ocean prior to landfall. Clear implications arise for AR data collection, identifying important regions which are not current examined where damaging ARs generate. The results presented aid in understanding the cause of damaging floods in the Western U.S. with the aim of supporting atmospheric river forecasts by linking atmospheric conditions to historic damage.

1. Introduction

Atmospheric rivers (ARs) are filamentary corridors of enhanced atmospheric water vapor transport that can produce extreme precipitation in mid-latitude regions, particularly when an AR undergoes ascent through interaction with topography (Zhu and Newell, 1998; Neiman et al., 2008). The magnitude and duration of the moisture flux directly relates to the intensity of precipitation with the highest precipitation rates being associated with strong, prolonged ARs (Konrad and Dettinger, 2017; Ralph et al., 2019; Eiras-Barca et al., 2021; Prince et al., 2021). Given the association between ARs and precipitation, the occurrence of ARs brings the potential for substantial environmental and socioeconomic impacts (Corringham et al., 2019). On the West Coast of the U.S., landfalling ARs are the primary cause of flooding with approximately 90% of all floods occurring during ARs (Dettinger et al., 2011; Paltan et al., 2017). The occurrence of these hydrological extremes often results in damage to property and infrastructure, a noteworthy event being the damage to the Oroville Dam in northern California resulting in mass evacuations and financial damages exceeding USD$1 billion (Vano et al., 2019; White et al., 2019). A primary mitigation of AR damage in the Northeast Pacific are operational reconnaissance campaigns, sampling ARs that impact the U.S. West Coast to improve forecasts of extreme precipitation (e.g. AR Recon, Ralph et al., 2020; Stone et al. 2020). AR Recon targets ARs at 1-5 days lead time (primarily between 180°W and the U.S. West Coast) and understanding the lifecycle (genesis and progression) and damage of ARs is important for identifying and sampling impactful ARs.

1.1 Atmospheric river damages

The financial cost of ARs in the Western U.S. was quantitatively examined by Corringham et al. (2019), demonstrating that over 84% of all flood losses are associated with ARs, exceeding 95% in coastal locations. The most extreme individual ARs are shown to exceed USD$3 billion in flood damages, with 13 ARs exceeding USD$1 billion over a 40-year period (Corringham et al., 2019). Furthermore, the majority of AR damage is shown to be attributed to a very small number of intense ARs with a distinct relationship between the magnitude and duration of AR and the experienced damage (Corringham et al., 2019). The financial cost of ARs has also been assessed in Europe, where ARs were found to account for 75% of the high-impact wind storms during 1997-2013, with extreme events exceeding USD$2 billion in damages in some cases (Waliser and Guan, 2017).

1.2 Atmospheric river lifecycle tracking

Rutz et al. (2020) highlights the importance of considering ARs through a Lagrangian perspective to understand their life cycle dynamics, specifying that automatic tracking of ARs in time and space has previously been a challenging endeavour. Recent advances in AR detection techniques (ARDTs) have allowed for the identification of full life cycle characteristics of ARs including the genesis location,

termination location, relative age, merging and separation (Zhou et al. 2018; Guan and Waliser, 2019; Zhou and Kim, 2019; Shearer et al. 2020). The study of AR life cycles remains as a key research gap identified as part of the AR Tracking Method Intercomparison Project (ARTMIP), a coordinated effort to quantify uncertainties in AR tracking and consequent conclusions (Shields et al., 2018; Rutz et al. 2019; O'Brian et al., 2020). Zhou and Kim (2019) have previously examined the impact and dynamics of AR genesis associated with the U.S. West Coast, finding that ARs with genesis locations in the Western Pacific (west of 170°W) tend to bring more rain to northern locations while Eastern Pacific ARs tend to bring rain to southern locations on the U.S. West Coast. Furthermore, it was also identified that ARs that travel further, from the Western Pacific, tend to have a higher IVT than ARs travelling from the Eastern Pacific (an approximate 30% increase) and last for longer (an average of approximately 2 days more; Payne and Magnusdottir, 2014; Zhou et al., 2018; Zhou and Kim, 2019).

This study provides crucial impact-based insight into the importance of AR genesis in the North Pacific basin through examining the relationship between genesis location and economic damage in the Western U.S. To do so, a lifecycle AR database is combined with estimates of daily economic damages. The synoptic-scale conditions during initiation of all ARs the most damaging ARs are also analyzed to probe the dynamics associated with these devastating events.

2. Data and methods

In this study, a database of daily AR occurrence along the U.S. West Coast is developed from the Guan and Waliser (2019) Version 3, Tracking Atmospheric Rivers Globally as Elongated Targets (tARget) algorithm (henceforth GW_{19}). The AR catalogue used herein was obtained by extracting unique AR ID values generated within GW_{19} which are consistent throughout an entire AR lifecycle. The GW_{19} catalogue was developed for the period between 1979 and 2019 (40 years) using 6-hourly instantaneous fields of global integrated vapor transport (IVT) at 1.5° resolution (the specified resolution of GW_{19}) from the ERA-Interim reanalysis (Dee et al., 2011). GW_{19} applies a series of magnitude and geometric threshold tests to identify elongated regions of elevated IVT. ARs at genesis are selected as the detected AR objects which do not have congruent or co-located ARs in the previous timestep, effectively the point in time when a region of IVT has become sufficiently large and intense to meet the geometric and magnitude thresholds for AR detection. The algorithm was first presented as a spatial feature identification technique (Guan and Waliser, 2015) and has since been evaluated and validated (Guan and Waliser, 2015; Guan and Waliser, 2018) and upgraded (optimized axis identification, iterative testing using variable IVT percentiles and exclusion of embedded tropical cyclones) with recent additions facilitating the temporal feature tracking of individual ARs, allowing for the characterisation of AR lifecycles (Guan et al., 2018; Guan and Waliser, 2019).

Landfalling ARs are detected as AR objects that intersect the coastline of North America defined by ERA-Interim at 1.5° resolution (Figure 1). The coastline is divided into 4 broad regions, Washington, Oregon/Northern California, California and Baja California to account for regional heterogeneities and circulation variability controlling AR propagation and landfall location as described by Guirguis et al. (2018) and Zhang and Villarini (2018). Over the 40-year study period, 4436 unique AR lifecycles made landfall on the U.S. West Coast. An annual mean of 36 AR events was recorded for all grid cells defining the U.S. West Coast (ranging between 32 and 44 ARs per year between grid cells), comparable to previously reported U.S. West Coast AR occurrence (Guan and Waliser, 2019).

Total estimated daily flood damages are calculated from the National Flood Insurance Program (NFIP; retrieved from the U.S. Federal Emergency Management Agency 2019) for a period between April 1979 and March 2019, spanning the same 40 year period as the AR catalogue. Only wintertime ARs (NDJFM) are analyzed and presented, aligning with the AR damage season as defined by Corringham et al. (2019), and all values are adjusted for inflation to 2020 USD. The insured losses are used as a proxy for total economic impact from floods based on Corringham et al. (2019) who calculated that total flood damages are approximately 30 times greater than reported NFIP-insured losses; a conversion used herein to report total economic damage.

In order to pair daily damage to AR occurrence, the 6-hourly AR catalogue is reduced to a daily resolution by selecting the AR object with the greatest landfalling IVT within each day (12% of ARs occurred simultaneously on the same day with higher IVT ARs along the coastline and were hence removed). Following daily aggregation, 3930 individual ARs remain, 15% (598) of which were excluded as spurious AR life cycles (ARs which only exist in a single time-step) to avoid possible double counting (following storm detection convention; Schreck et al., 2014). The final database consists of 3332 individual AR lifecycles that made landfall on the U.S. West Coast over the 40-year period (mean annual occurrence of 83 per year across the entire coastline). The landfall location for each AR is recorded as the location which receives the maximum onshore IVT; for example, 1367 ARs were recorded to experience maximum IVT in Washington, or approximately 34 per year. Following identification of AR genesis locations based on economic impact, the atmospheric dynamics associated with AR genesis are assessed. Geopotential height at 500 hPa, integrated vapor transport (IVT) and the 300 hPa zonal wind at 1.5° resolution and 6-hourly time steps are retrieved from the ERA-Interim reanalysis to observe the atmospheric conditions during genesis.

3. Results and Discussion

The total accumulated flood damage over this period was $51.0 billion, with ARs accounting for 86% of these damages ($44.1 billion). Annually, ARs account for an average of 88% of flood insurance claims with an annual mean AR damage of $1.1 billion. The proportion of flood damage from ARs is

greater nearer to the coast, with California, Nevada, Oregon, and Washington all receiving over 90% of the mean annual flood damage during ARs (Figure 1). The greatest total and AR-related damages are recorded in California where ARs cause an average $657 million of flood damage annually. The proximity to the coastline, adjacent topographic barriers, population density, risk of infrastructure and habitation of flood plains collectively contribute to this comparatively large economic impact (Dettinger et al., 2011).

The proportion of damage in each state broadly aligns with the landfall location (Figure 1), with the majority of damage generally arising from ARs that make landfall on the adjacent coastline. The AR damage recorded in each state is recorded as the damage that occurs on the day and day following an AR is detected anywhere along the coastline (consistent with Corringham et al., 2019). Notably, the highest proportion of AR damage in Arizona, New Mexico, Colorado and Utah arise from ARs that make landfall in Baja California. Rutz and Steenburgh (2012) and Neiman et al. (2013) proposed suitable explanations for extreme precipitation in the southern semiarid region of the Western U.S., describing the region of low topography between northern Baja California and the Sierra Madre Occidental as a suitable corridor for inland penetration of ARs without prior orographic forcing. Some anomalies exist, such as the greatest proportion of flood damage in Nevada coming from ARs that make landfall in Washington. One explanation may be due to migration of landfall location over the full lifecycle of the event, or from simultaneous flooding at both locations due to different weather events (12% of ARs made landfall simultaneously with greater magnitude ARs and subsequently excluded from analysis). The landfall location (here considered as the location of maximum IVT) does not account for initial or shifting landfall locations through the progression of AR, but rather represents the location where the AR would be expected to be most impactful.

3.1 Atmospheric river genesis location based on financial impact

The genesis frequency of ARs that make landfall on the U.S. West Coast is shown in Figure 2 (separated by landfall region as defined in Figure 1). The frequency is calculated as the number of times an AR object has a genesis stage in each grid cell divided by the total number of ARs which make landfall for each region in the U.S. West Coast. The units can be interpreted as a conditional frequency; i.e., given that an AR makes landfall within each region, what is the frequency of genesis AR objects at each grid cell?

AR genesis is more regionally constrained for southern regions, with all ARs that make landfall in Baja California having genesis locations centred around 25°N, immediately over the landmass of Baja California. This region has been previously identified as a key region for AR genesis with ARs propagating to the northeast towards the North Atlantic Ocean, aligning with the predominant northeast moisture advection (Zhang and Villarini, 2018; Guan and Waliser, 2019). When considering damaging

ARs (75th percentile) landfalling in Baja California, there is a westward shift offshore with reduced genesis frequency over the landmass of North America and an absolute increase in genesis frequency of 10% over the ocean adjacent to Baja California (statistically significant, at the 90% level from a one-sided Fisher-exact test).

The genesis location of ARs that make landfall in California extends further westward in the Pacific Ocean than Baja California ARs, with elevated genesis frequencies above 5% extending to Hawaii. There is a southwest shift in damaging (75th percentile) California ARs, with statistically significant absolute increases in genesis frequency up to 10% centred between Hawaii and the Californian coastline (140°W). Oregon/North California and Washington both exhibit similar distributions of AR genesis, with elevated genesis frequencies extending west across the entire North Pacific basin towards southern Japan (140°E). AR genesis is primarily centred along 30°N with a northward curve in genesis locations approaching the coastline of North America (eastward of Hawaii). Damaging ARs in these two regions have increased genesis frequencies in the Central and Western Pacific basin with substantial increases in AR frequency westward of 180°W. This region of elevated AR frequency is similar to the definition of Western Pacific AR genesis as defined by Zhou and Kim (2019). Presented here is the first documentation of AR genesis locations for the U.S. West Coast, differentiated by region and damage following landfall.

There is a broad westward shift in AR genesis location (genesis object centroid location) as damage percentile increases for all regions, with the largest shift occurring in the northern two regions (Oregon/Northern California and Washington; Figure 3 and S1). Generally, ARs that make landfall further north on the U.S. West Coast tend to have genesis further west, with over 25° longitude difference between the median AR genesis centroid location for Washington compared to the Oregon/Northern California region. The median longitude of AR genesis shifts between 8° and 27° westward when considering the most damaging ARs (90th percentile of damage) compared to all ARs. The median landfalling AR IVT also increases with damage percentile level; ARs that cause damage in the 90th percentile have a median landfalling IVT 224 to 369 kg m^{-1} s^{-1} greater than the median landfalling IVT of the full AR dataset (increases of 57% to 82%).

Corringham et al. (2019) quantified the relationship between financial cost and AR IVT, demonstrating that higher IVT is associated with increasing damages in a near exponential relationship (validated here in Figure S2). The results presented here are in agreement, with higher IVT providing a suitable explanation for why these ARs are more damaging, with many studies identifying the intrinsic relationship between AR IVT and precipitation/flooding (Neiman et al., 2009; Konrad and Dettinger 2017; Ralph et al., 2019). ARs from the Western Pacific tend to have a higher IVT and persist for longer compared to Eastern Pacific ARs (Zhou et al., 2018; Zhou and Kim 2019). Payne and Magnusdottir (2014) discussed that the enhanced zonal winds that allow for propagation of ARs from further across

the Pacific may be the reason why these ARs tend to also have elevated moisture fluxes. Scavenging of water vapor along the AR track may also occur, as moisture from previous cyclonic and frontal systems may converge and intensify a migrating AR (Sodemann and Stohl, 2013; Sodemann et al., 2020). Crucially, the results presented here demonstrate that AR landfalling IVT tends to increase with genesis distance from landfall, regardless of the location within the Pacific Ocean. There is not a particular location where damaging ARs have genesis, but rather, damaging ARs have genesis further from landfall compared to the distribution of all ARs that make landfall for each region.

3.2 Atmospheric conditions at genesis

The position of the AR genesis low pressure anomaly appears as the dominant driver for controlling the location of landfall (Figure 4a, S3). Zhang et al. (2019) found that about 82% of ARs are associated with extratropical cyclones (ECs) and while ECs are not objectively identified in this study, the composite atmospheric conditions during AR genesis certainly indicate that AR genesis is generally associated with EC activity. For Washington, the low pressure anomaly is centred in the Gulf of Alaska with the centre of the anomaly shifting southeast for each region southward down the U.S West Coast. The position of the genesis low pressure anomaly close to the coastline appears similar to previously presented landfalling anomalies for each location (Guirguis et al., 2018), which may be attributed to the majority of ARs that have genesis locations reasonably close to the coastline (Figure 2). Another point of interest regarding the position of all AR genesis is the increasing size and magnitude of the high pressure anomaly on the northwest side of the low pressure anomaly (in the Gulf of Alaska) for ARs making landfall further south, suggesting that ridging may be more persistent during genesis of ARs that landfall on the southern U.S. West Coast. The IVT vector anomaly demonstrates the broad elevated geostrophic flow directed towards the coastline on the south/southeast edge of the low pressure anomaly. In California and Baja California there is also a substantial counterflow anomaly on the northwest edge of the low pressure associated with the more established dipole pressure anomaly. The elevated IVT vector anomalies are also colocated with elevated 300hPa zonal wind anomalies.

When considering the subset of damaging ARs (75^{th} percentile) the magnitude of the pressure anomalies become greater along with larger regions of elevated IVT extending further westward across the Pacific (Figure 4a). The magnitude of the 300hPa zonal wind anomaly is also greater for these damaging ARs and generally covers a larger area, most notably for Oregon/Northern California where the zonal wind anomaly extends zonally across the entire north Pacific basin. The high pressure anomalies are also more prevalent for damaging ARs. Lower EC pressures have been previously associated with AR IVT intensity (e.g. Zhang et al., 2019) and the results presented here directly links the magnitude of the low pressure anomaly at AR genesis to increased economic impact following landfall.

Figure 4b presents the same atmospheric composites and anomalies as Figure 4a, but for the subset of ARs with genesis locations in the western region of the north Pacific basin as defined by Zhou and Kim (2019, westward of 170°W). The pressure anomalies are much larger than Figure 4a with a broad zonally extended low pressure region spanning the north Pacific basin, possibly exhibiting the progression of multiple ECs, particularly for the most damaging ARs in Oregon/Northern California that originate from the Western Pacific. This suggestive waveguide is similar to those presented by Fish et al. (2019) when identifying AR families; ARs making landfall in rapid succession. Cordeira et al. (2013) provides an example of an AR that caused flooding in the Western U.S. which originates off the coast of Japan, demonstrating that multiple cyclonic systems may be associated with the progression of a single AR from the Western Pacific (discussed further in Sodemann et al., 2020).The elevated IVT extending throughout the entire Pacific also suggests that at the point of AR genesis in the western Pacific, there are elevated moisture fluxes downstream (possible concurrent ARs) already making landfall on the U.S. West Coast. The zonally extended 300hPa jet stream (with a maximum zonal core at 35°N) observed in Figure 4b is also congruent with findings from Cordeira et al. (2013), Payne and Magnusdottir (2014) and Fish et al. (2019), allowing for the zonal propagation of ECs and associated ARs across the entire Pacific, also suggesting that the occurrence of damaging ARs from the West Pacific may be associated with the rapid progression of multiple ARs (i.e. an AR family).

4. Conclusions

ARs account for 88% of annual total flood damages in the Western U.S., causing on average $1.1 billion of damage annually. Presented here is the initial examination linking AR flood damage to atmospheric dynamics through a study of AR genesis. ARs that cause substantial economic impact to the Western U.S. are unique in both their lifecycle and magnitude, with the most impactful events tending to originate from further across the ocean prior to landfall paired with a substantially higher moisture flux at landfall. ARs that cause extreme damage (90^{th} percentile) tend to have genesis locations between 8° and 27° longitude further westward and IVT increases of 57% to 82% compared to all ARs that make landfall on the U.S. West Coast. The relationship found between AR impacts and genesis location will help inform targeted deployment of future observation campaigns (AR Recon). Due to the relative importance of West Pacific ARs, there may be a possibility to improve longer lead forecasts of extreme precipitation by observing ARs at genesis in these westward locations, a region not currently considered for AR Recon. Linking AR dynamics and lifecycle to economic impact also provides an opportunity to explore impact-based AR forecasting along with facilitating the study of how changing atmospheric dynamics in the Pacific Ocean may influence flood damages experienced in the Western U.S.

Data availability statement

The AR data are available at https://ucla.box.com/ARcatalog. Development of the AR detection algorithm and databases was supported by NASA. AR detection is based on the algorithm originally introduced in Guan and Waliser (2015), refined in Guan et al. (2018), and further enhanced in Guan and Waliser (2019) with tracking capability. Flood damages in the Western U.S. were retrieved through the National Flood Insurance Program retrieved from the U.S. Federal Emergency Management Agency, downloaded 2019-10-25 (https://www.fema.gov/openfema-data-page/fima-nfip-redacted-claims-v1).

References

Corringham, T. W., Ralph, F. M., Gershunov, A., Cayan, D. R. and Talbot, C. A. (2019). Atmospheric rivers drive flood damages in the western United States. *Science Advances*, 5(12), 1-7. https://doi.org/10.1126/sciadv.aax4631

Dee, D. P., Uppala, S. M., Simmons, A. J., Berrisford, P., Poli, P., Kobayashi, S., et al. (2011). The ERA-Interim reanalysis: Configuration and performance of the data assimilation system. *Quarterly Journal of the Royal Meteorological Society*, 137(656), 553–597. https://doi.org/10.1002/qj.828

Dettinger, M. D., Ralph, F. M., Das, T., Neiman, P. J. and Cayan, D. R. (2011). Atmospheric rivers, floods and the water resources of California. *Water*, 3, 445–478. https://doi.org/10.3390/w3020445

Eiras-Barca, J., Ramos, A. M., Algarra, I., Vázquez, M., Dominguez, F., Miguez-Macho, G., et al. (2021). European West Coast atmospheric rivers: A scale to characterize strength and impacts. *Weather and Climate Extremes*, 31, p.100305. https://doi.org/10.1016/j.wace.2021.100305

Fish, M. A., Wilson, A. M. and Ralph, F. M. (2019). Atmospheric river families: Definition and associated synoptic conditions. *Journal of Hydrometeorology*, 20(10), 2091-2108. https://doi.org/10.1175/JHM-D-18-0217.1

Guan, B. and Waliser, D. E. (2015). Detection of atmospheric rivers: Evaluation and application of an algorithm for global studies. *Journal of Geophysical Research: Atmospheres*, 120, 12,514-12,535. https://doi.org/10.1002/2015JD024257

Guan, B. and Waliser, D. E. (2017). Atmospheric rivers in 20 year weather and climate simulations: A multimodel, global evaluation, *Journal of Geophysical Research: Atmospheres*, 122, 5556–5581, https://doi.org/10.1002/2016JD026174

Guan, B. and Waliser, D. E. (2019). Tracking Atmospheric Rivers Globally: Spatial Distributions and Temporal Evolution of Life Cycle Characteristics. *Journal of Geophysical Research: Atmospheres*, 124, https://doi.org/10.1029/2019JD031205

Guan, B., Waliser, D. E. and Ralph, F. M. (2018). An intercomparison between reanalysis and dropsonde observations of the total water vapor transport in individual atmospheric rivers. *Journal of Hydrometeorology*, 19(2), 321-337. https://doi.org/10.1175/JHM-D-17-0114.1

Guirguis, K., Gershunov, A., Clemesha, R. E. S., Shulgina, T., Subramanian, A. C., and Ralph, F. M. (2018). Circulation drivers of atmospheric rivers at the North American West Coast. *Geophysical Research Letters*, 45, 12,576–12,584. https://doi.org/10.1029/2018GL079249

Konrad, C. P. and Dettinger, M. D. (2017). Flood runoff in relation to water vapor transport by atmospheric rivers over the western United States, 1949–2015. *Geophysical Research Letters*, 44, 11,456–11,462. https://doi.org/10.1002/ 2017GL075399

Neiman, P. J., Ralph, F. M., Moore, B. J., Hughes, M., Mahoney, K. M., Cordiera, J. M. and Dettinger, M. D. (2013). The landfall and inland penetration of a flood-producing atmospheric river in Arizona. Part I: Observed synoptic-Scale, orographic, and hydrometeorological characteristics. *Journal of Hydrometeorology*, 14(2), 460-484. https://doi.org/10.1175/JHM-D-12-0101.1

Neiman, P. J., Ralph, F. M., Wick, G. A., Lundquist, J. D. and Dettinger, M. D. (2008). Meteorological characteristics and overland precipitation impacts of atmospheric rivers affecting the West Coast of North America based on eight years of SSM/I satellite observations. *Journal of Hydrometeorology*, 9, 22-47. https://doi.org/10.1175/2007JHM855.1

Neiman, P. J., White, A. B., Ralph, F. M., Gottas, D. J. and Gutman, S. I. (2009). A water vapour flux tool for precipitation forecasting. *Proceedings of the Institution of Civil Engineers Water Management* (162, WM2). 83–94. https://doi.org/10.1680/wama.2009.162.2.83

O'Brian, T., Payne, A. E., Shields, C. A., Rutz, J., Brands, S., Castellano, C. et al. (2020). Detection uncertainty matters for understanding atmospheric rivers. *Bulletin of the American Meteorological Society, Meeting Summary*, E790–E796. https://doi.org/10.1175/BAMS-D-19-0348.1

Paltan, H., Waliser, D., Lim, W. H., Guan, B., Yamazaki, D., Pant, R., and Dadson, S. (2017). Global floods and water availability driven by atmospheric rivers. *Geophysical Research Letters*, 44, 10,387–10,395. https://doi.org/10.1002/ 2017GL074882

Payne, A. E. and Magnusdottir, G. (2014). Dynamics of Landfalling Atmospheric Rivers over the North Pacific in 30 Years of MERRA Reanalysis. *Journal of Climate*, 27(18), 7133-7150. https://doi.org/10.1175/JCLI-D-14-00034.1

Prince, H. D., Cullen, N. J., Gibson, P. B., Conway, J. and Kingston, D. G. (2021). A climatology of atmospheric rivers in New Zealand. *Journal of Climate*, Early Online Release, 1-56. https://doi.org/10.1175/JCLI-D-20-0664.1

Ralph, F. M., Rutz, J. J., Cordeira, J. M., Dettinger, M., Anderson, M., Reynolds, D., Schick, L. J. and Smallcomb, C. (2019). A scale to characterize the strength and impacts of atmospheric rivers. *Bulletin of the American Meteorological Society*, 100(2), 269-289. https://doi.org/10.1175/BAMS-D-18-0023.1

Rutz, J. J., and Steenburgh, W. J. (2012). Quantifying the role of atmospheric rivers in the interior western United States. *Atmospheric Science Letters*, 13, 257–261, https://doi.org/10.1002/asl.392

Rutz, J. J., Guan, B., Bozkurt, D., Valenzuela, R., Gorodetskaya, I. V., Gershunov, A. et al. (2020). 'Global and Regional Perspectives', Ralph, F. M. (eds), *Atmospheric Rivers*, Springer Nature, Switzerland, 89-140. https://doi.org/10.1007/978-3-030-28906-5_4

Rutz, J. J., Shields, C. A., Lora, J. M., Payne, A. E., Guan, B., Ullrich, P. et al. (2019), The Atmospheric River Tracking Method Intercomparison Project (ARTMIP): Quantifying uncertainties in atmospheric river climatology, *Journal of Geophysical Research: Atmospheres*, 124, 13777–13802, https://doi.org/10.1029/2019JD030936

Schreck, C. J. III, Knapp, K. R. and Kossin, J. P. (2014). The impact of best track discrepancies on global tropical cyclone climatologies using IBTrACS. *Monthly Weather Review*, 142(10), 3881-3899. https://doi.org/10.1175/MWR-D-14-00021.1

Shearer, E. J., Nguyen, P., Sellars, S. L., Analui, B., Kawzenuk, B., Hsu, K., et al. (2020). Examination of global midlatitude atmospheric river lifecycles using an object-oriented methodology. *Journal of Geophysical Research: Atmospheres*, 125, e2020JD033425. https://doi.org/10.1029/2020JD033425

Shields, C. A., Rutz, J. J., Leung, L.-Y., Ralph, F. M., Wehner, M., Kawzenuk, B. et al. (2018). Atmospheric River Tracking Method Intercomparison Project (ARTMIP): Project goals and experimental design. *Geoscientific Model Development*, 11, 2455–2474. https://doi.org/10.5194/gmd-11-2455-2018

Sodemann, H., and Stohl, A. (2013). Moisture origin and meridional transport in atmospheric rivers and their association with multiple cyclones. *Monthly Weather Review*, 141, 2850–2868. https://doi.org/10.1175/MWR-D-12-00256.1

Sodemann, H., Wernli, H., Knippertz, P., Cordeira, J. M., Dominguez, F., Guan, B. et al. (2020). 'Structure, Process and Mechanism', Ralph, F. M. (eds), *Atmospheric Rivers*, Springer Nature, Switzerland, 15-43. https://doi.org/10.1007/978-3-030-28906-5_2

Vano, J. A., Miller, K., Dettinger, M. D., Cifelli, R., Curtis, D., Dufour, A., Olsen, J. R. and Wilson, A. M. (2019). Hydroclimatic extremes as challenges for the water management community: Lessons from Oroville Dam and hurricane Harvey. *Bulletin of the American Meteorological Society*, 100, S9–S14. https://doi.org/10.1175/BAMS-D-18-0219.1

Waliser, D. and Guan, B. (2017). Extreme winds and precipitation during landfall of atmospheric rivers. *Nature Geoscience*, 10, 179–183 https://doi.org/10.1038/NGEO2894

White, A. B., Moore, B. J., Gottas, D. J., Neiman P. J. (2019). Winter storm conditions leading to excessive runoff above California's Oroville Dam during January and February 2017. *Bulletin of the American Meteorological Society*, 100, 55–70. https://doi.org/10.1175/BAMS-D-18-0091.1

Zhang, Z., Ralph, F. M., and Zheng, M. (2019). The relationship between extratropical cyclone strength and atmospheric river intensity and position. *Geophysical Research Letters*, 46, 1814–1823. https://doi.org/10.1029/ 2018GL079071

Zhou, Y., and Kim, H. (2019). Impact of Distinct Origin Locations on the Life Cycles of Landfalling Atmospheric Rivers Over the U.S. West Coast. *Journal of Geophysical Research: Atmospheres*, 124, 11,897–11,909. https://doi.org/10.1029/2019JD031218

Zhou, Y., Kim, H., and Guan, B. (2018). Life cycle of atmospheric rivers: Identification and climatological characteristics. *Journal of Geophysical Research: Atmospheres*, 123, 12,715–12,725. https://doi.org/10.1029/ 2018JD029180

Zhu, Y. and Newell, R. E. (1994). Atmospheric rivers and bombs. *Geophysical Research Letters*, 21(18), 1999-2002. https://doi.org/10.1029/94GL01710

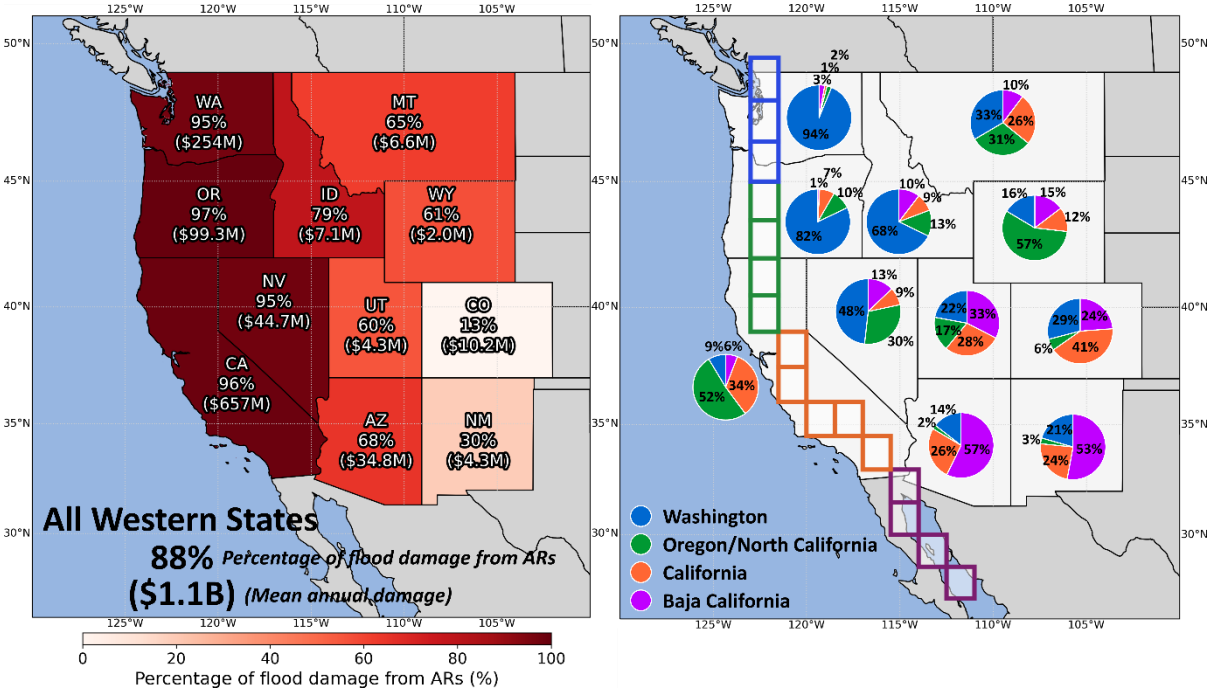

Figure 1. (left) The percentage of mean annual flood damage in the Western continental U.S. by state, caused by ARs with the resulting mean annual cost of ARs shown in parentheses. (right) The coastline of the Western U.S. is divided into four broad regions (Washington - blue, Oregon/North California - green, California - orange and Baja California - purple) to study the genesis locations of ARs that make landfall in different locations. The proportion of damage in each state caused by landfalling ARs from each portion of coastline is shown in the pie charts.

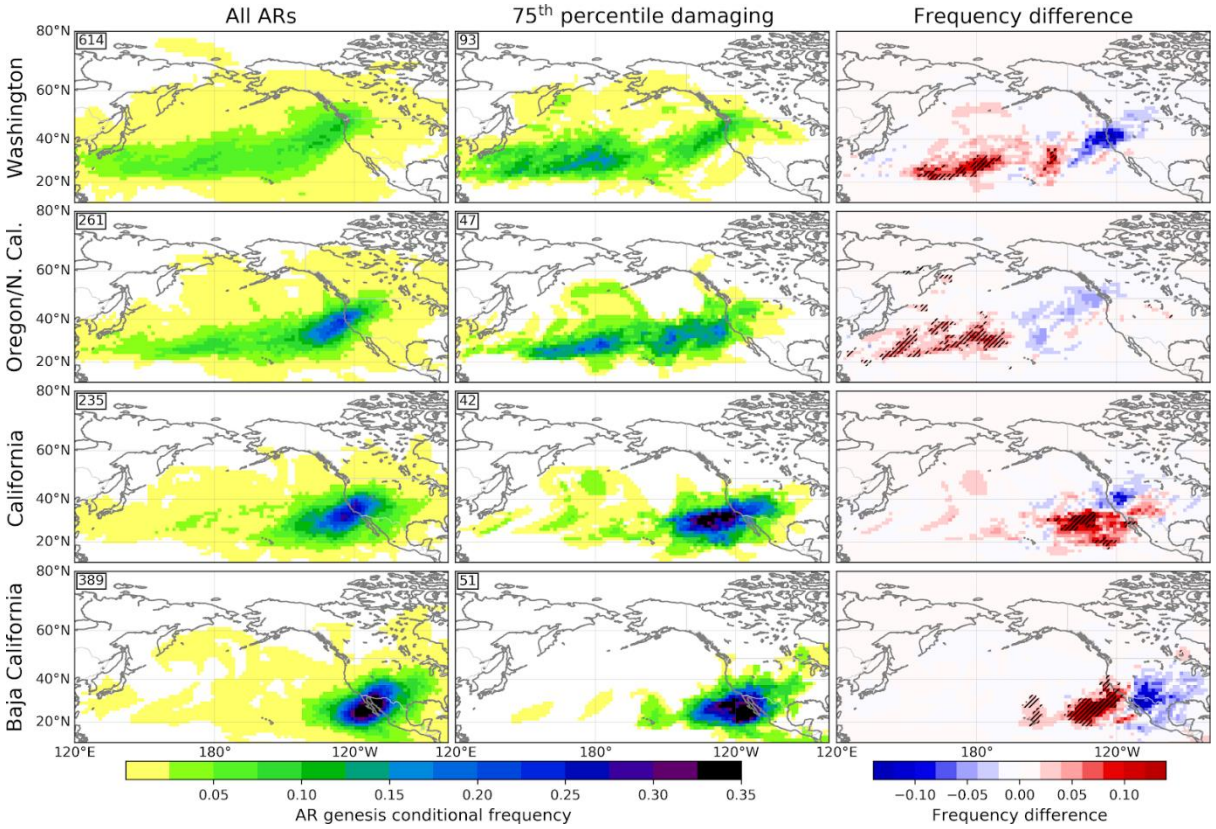

406 **Figure 2.** Conditional frequency of AR genesis for ARs making landfall in the four regions defined in Figure 1
407 for all landfalling ARs (left) and those that produce damage in the 75th percentile (centre). Conditional frequency
408 is the probability an AR object originates from a grid cell given that it makes landfall in each location and causes
409 damage in the specified range (i.e. exceeding the 75th percentile). The numerical absolute increase in frequency is
410 shown (right) with statistical significance ($p<0.1$) shown with dashed lines (from a one-sided Fisher-exact test).

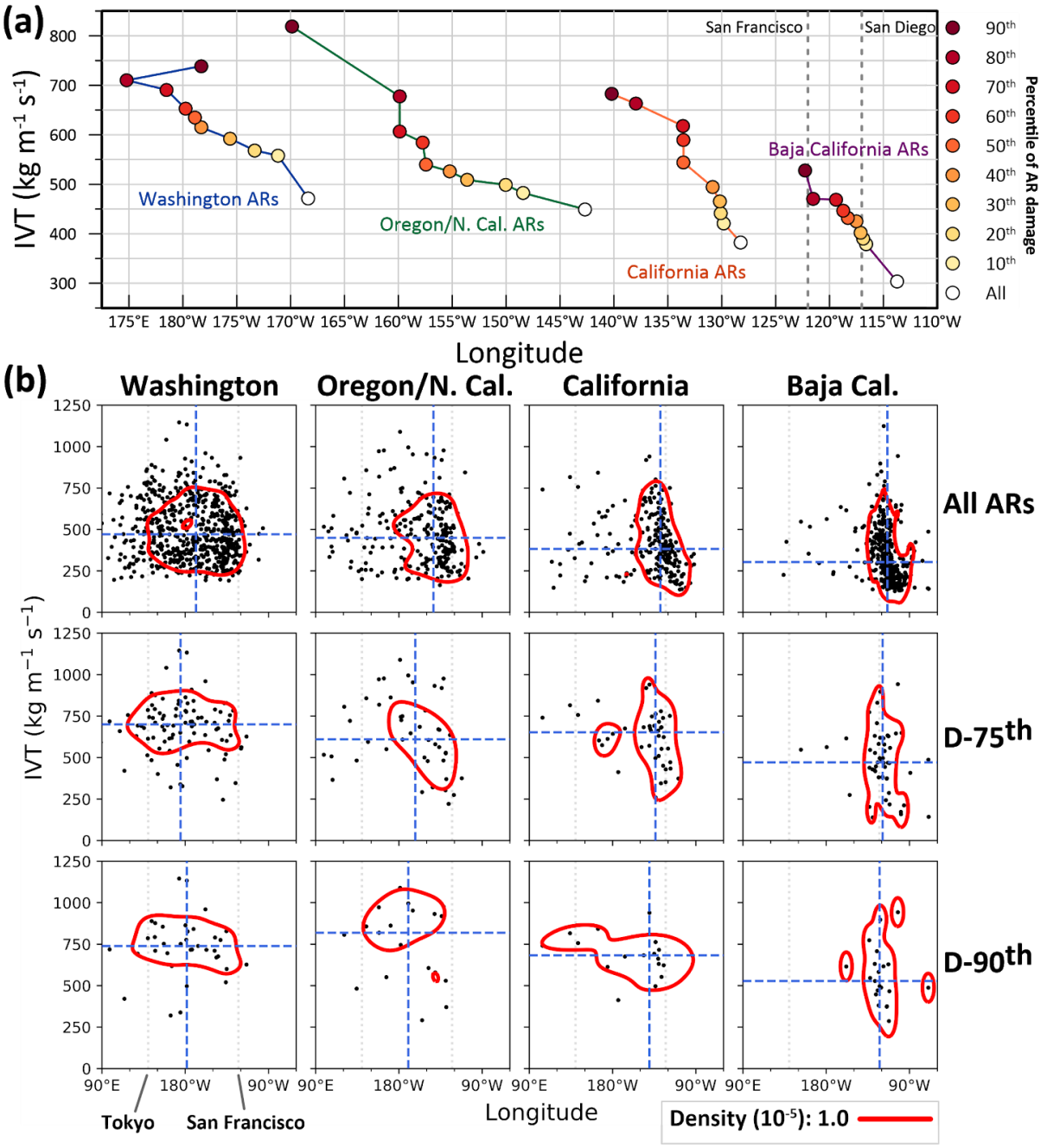

Figure 3. (a) Median AR genesis longitude and landfalling IVT for different damage percentiles for each region. Data points coloured for each percentile level, white to red, with white dots representing the full AR database both damaging and non-damaging. The longitude of San Francisco and San Diego are shown with the grey dotted lines to give context of the U.S. West Coast. (b) The distribution of AR genesis longitude and landfalling IVT for all ARs, ARs that cause damage in the 75th percentile (D-75th) and ARs that cause damage in the 90th percentile (D-90th). Density shown in red as calculated with KDE (gaussian filter and Scott's bandwidth). The median of each distribution is shown with the blue dotted lines and the location of Tokyo and San Francisco shown with light grey dotted lines to provide context of the North Pacific basin.

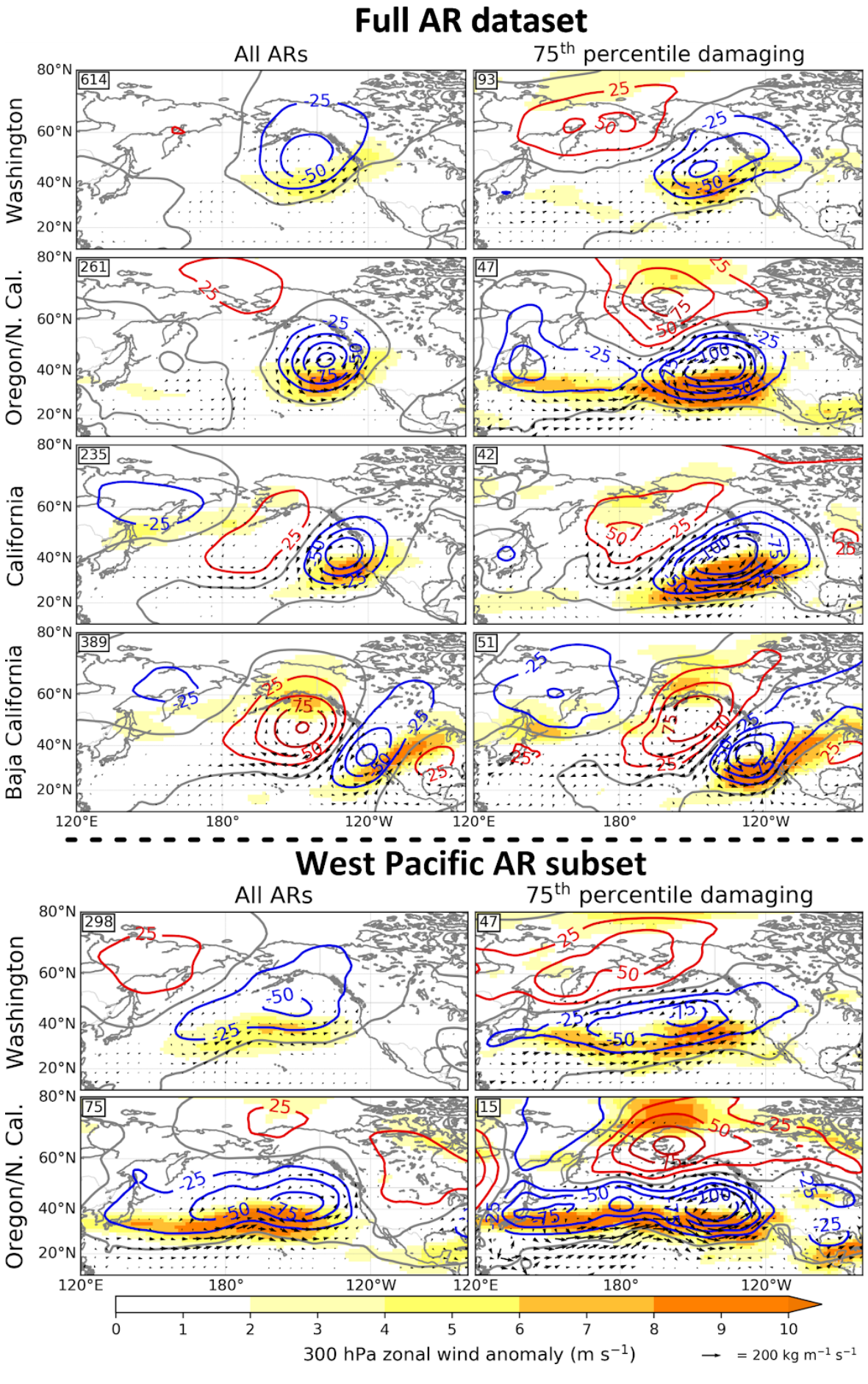
Full AR dataset
All ARs
75th percentile damaging
Washington
Oregon/N. Cal.
California
Baja California
614
93
261
47
235
42
389
51
80°N
60°N
40°N
20°N
120°E
180°
120°W
West Pacific AR subset
All ARs
75th percentile damaging
298
47
75
15
0 1 2 3 4 5 6 7 8 9 10
300 hPa zonal wind anomaly (m s−1)
= 200 kg m−1 s−1

Figure 4. Atmospheric conditions at the time of AR genesis shown with composites of anomalous 6-hourly Z500 (red/blue 25 m contours for positive/negative anomalies, zero line shown in grey), 300hPa zonal wind anomaly (orange shading) and IVT vector anomaly (vector magnitude greater than 15 kg $m^{-1}s^{-1}$). Composites at the time of genesis are shown for (left) all landfalling ARs and (right) ARs that produce damage in the 75th percentile. The number of AR genesis events considered for each plot is shown in the top left corner. A subset of ARs with genesis locations in the Northwest Pacific Ocean (west of 170°W) are shown for Oregon/N. Cal. And Washington in the lower plot.